

SUPPLEMENTARY INFORMATION

Polar jets of swimming bacteria condensed by a patterned liquid crystal

Taras Turiv¹, Runa Koizumi¹, Kristian Thijssen², Mikhail M. Genkin³, Hao Yu¹, Chenhui Peng¹, Qi-Huo Wei^{1,4}, Julia M. Yeomans², Igor S. Aranson⁵, Amin Doostmohammadi², Oleg D. Lavrentovich^{1,4*}

Affiliation:

¹*Advanced Materials Liquid Crystal Institute and Chemical Physics Interdisciplinary Program, Kent State University, Kent, OH 44242, USA*

²*The Rudolf Peierls Centre for Theoretical Physics, University of Oxford, Clarendon Laboratory, Parks Rd., Oxford, OX1 3PU, UK*

³*Cold Spring Harbor Laboratory, 1 Bungtown Rd, Cold Spring Harbor, NY 11724, USA*

⁴*Department of Physics, Kent State University, Kent, OH 44242, USA*

⁵*Department of Biomedical Engineering, Pennsylvania State University, University Park, Pennsylvania 16802, USA*

Corresponding author:

*Author for correspondence: e-mail: olavrent@kent.edu, tel.: +1-330-672-4844.

Keywords: active matter, liquid crystals, living bacteria

Supplementary text

Realignment of a bacterium away from the director of the surrounding nematic. A bacterium such as *B. subtilis* can develop a realigning torque $\tau_{\text{bact}} \approx \beta U_0$, where β is the angle between the bacterial body axis and the local $\hat{\mathbf{n}}_0$, $U_0 = f_{\text{thrust}} l_D$ is the hydrodynamic force dipole strength, f_{thrust} is the thrust force, and l_D is the length of the force dipole associated with the force-free mode of locomotion. In the order of magnitude for bacteria swimming in water¹, $\tau_{\text{bact}} / \beta \approx (1 - 10) \times 10^{-18}$ N m; τ_{bact} in a nematic medium is expected to be of a similar order of magnitude, but can also be somewhat larger because of an increased l_D ². The stabilizing torque of the surrounding nematic on a bacterium attempting a realignment comes from the elastic distortions and from finite strength of the surface anchoring of the director at the bacterial body. The elastic torque, calculated by Smith and Denniston³ for a rod of length l and radius r with an infinitely strong anchoring at its surface, realigned by an angle β from $\hat{\mathbf{n}}_0$, is $\tau_{\text{el}} \approx \beta C K l$, where $C \approx 4\pi / \ln(2l/r)$. For the typical $K = 10$ pN⁴, $l = 8$ μm , $r = 0.4$ μm , one finds $\tau_{\text{el}} / \beta \approx 3 \times 10^{-16}$ N m, a value much higher than $\tau_{\text{bact}} / \beta$, which makes it difficult for a bacterium to realign. Of course, the assumption of infinite surface anchoring must be mitigated and the surface energy penalty for the bacterial realignment with respect to $\hat{\mathbf{n}}_0$ should be finite, $w_b \beta^2 / 2$, where w_b is the surface anchoring strength at the bacterial body¹, expected to be on the order of 10^{-6} J/m² or even less⁵⁻⁷. The corresponding stabilizing anchoring torque is then reduced to $\tau_{\text{surf}} / \beta \approx 2\pi r l w_b \approx (10 - 20) \times 10^{-18}$ N m, comparable but still typically larger than the bacterial realigning torque. These estimates are in line with the experimental observation that the preferred direction of an individual swimming bacterium is parallel to the local $\hat{\mathbf{n}}_0$.

Reversal time of the bacteria swimming direction. The probability for the bacteria to reverse the direction of motion is calculated as the ratio of the number of reversal events to the total number of bacteria swimming through the patterned director field over the period of $\Delta t = 60$ s (Supplementary Video 1). The reversal probability $p_0 \sim 5 \times 10^{-3}$ is then calculated for three

intervals, each of time interval Δt and averaged. The experimental reversal time of the bacteria swimming direction was then calculated as $\tau = \Delta t / p_0 \sim 1.2 \times 10^4$ s .

Advection-diffusion analytical model for a living nematic. The constants c^\pm in equation (5) can be determined from the following consideration. According to the definition, a population c^+ swims parallel to \hat{n}_0 , and c^- swims antiparallel. Thus, the direction of motion of c^+ and c^- alternates between the neighboring bands. Because of these alternations, c^+ in one band travels in the same direction as c^- in the neighboring band (e.g. from left to right). This makes it possible to construct a nematic L -periodic solution rather than a $2L$ -periodic solution corresponding to the periodicity of the vector field \hat{n}_0 . Assuming $c^+(y) = c^-(y + L)$, we find $c^+ = c^- = c_0 / 2$. Note that c_0 has a dimension of bacterial concentration (m^{-3}). However, because c_0 in Eq. (4) and (5) serves merely as an integration/normalization constant, it typically attains very small values, on the order 10^{-8} m^{-3} , many orders of magnitude smaller than the average bacterial concentration.

For a better comparison with experiment, it is useful to introduce the concentrations c^{right} , c^{left} of bacteria traveling strictly right and left, respectively. To do that, we need to relabel the concentrations of c^\pm of bacteria traveling parallel/antiparallel to \hat{n}_0 because \hat{n}_0 alternates signs between the splay bands. Thus, we define

$$\begin{aligned} c^{\text{left}} &= c^- \text{ and } c^{\text{right}} = c^+ \text{ if } \cos(ky) > 0; \\ c^{\text{left}} &= c^+ \text{ and } c^{\text{right}} = c^- \text{ if } \cos(ky) < 0. \end{aligned} \quad (7)$$

Here $k = \pi / L$. The corresponding plots of c^{right} and c^{left} are shown in Supplementary Fig. S1a.

Effect of bacterial activity on director anchoring. Consider the prescribed pattern $\hat{n}_0 = [\cos(ky), -\sin(ky)]$; we omit the zero z -component. Activity of bacteria creates an active stress^{7,8,13} $\sigma_{\text{act}} = -U_0 \mathbf{Q} (c^+ + c^-)$, \mathbf{Q} is the tensorial order parameter

$$\mathbf{Q} = \begin{pmatrix} n_x^2 - 1/2 & n_x n_y \\ n_x n_y & n_y^2 - 1/2 \end{pmatrix} = \frac{1}{2} \begin{pmatrix} \cos(2ky) & -\sin(2ky) \\ -\sin(2ky) & -\cos(2ky) \end{pmatrix}, \quad (8)$$

where n_x and n_y are the components of the actual director $\hat{\mathbf{n}}$ that might be different from $\hat{\mathbf{n}}_0$. Associated with the active stress there is a force $\mathbf{F} = \nabla \cdot \boldsymbol{\sigma}_{\text{act}}$ that affects the director. In the Landau-Lifshitz-Gilbert form (to ensure $\hat{\mathbf{n}}^2 = 1$), a relaxation equation for the nematic director is $\partial_t \hat{\mathbf{n}} = -\hat{\mathbf{n}} \times \hat{\mathbf{n}} \times (a \hat{\mathbf{n}} + 2\gamma \mathbf{F})$. Here a is the director relaxation rate which depends on the in-plane director anchoring strength w_s at the bounding substrates and γ is a coefficient which depends on the anchoring strength w_b at the bacterial body. In the steady state, $\hat{\mathbf{n}} = (\hat{\mathbf{n}}_0 + 2\gamma \mathbf{F} / a) / |(\hat{\mathbf{n}}_0 + 2\gamma \mathbf{F} / a)|$. We consider only the y -component since there is no x -dependence. Since in the splay region $\gamma |\mathbf{F}| / a \ll 1$, $|n_y| \ll |n_x| \approx 1$, we obtain in the first order in F_y, n_y :

$$n_y \approx n_y^0 + \frac{2\gamma}{a} F_y \approx -\sin(ky) + \frac{\gamma U_0}{a} \partial_y \left[(c^+ + c^-) \cos(2ky) \right] \quad (9)$$

For an infinite reversal time τ , the equations for c^\pm become decoupled and in the corresponding splay bands we can use only c^+ or c^- . Consider for the definiteness the band where $c^- = 0$ and only c^+ is present. From Eq. (3) of the main text, we obtain a nonlinear ordinary differential equation

$$v_0 c^+ \left\{ -\sin(ky) + \frac{\gamma U_0}{a} \partial_y \left[c^+ \cos(2ky) \right] \right\} = D_c \partial_y c^+. \quad (10)$$

This equation can be integrated explicitly in terms of the Lambert W function

$$c^+ = - \frac{W \left\{ -\frac{\gamma v_0 U_0}{a D_c} C^+ \exp \left[\frac{v_0 L}{\pi D_c} \cos(ky) \right] \cos(2ky) \right\}}{\frac{\gamma v_0 U_0}{a D_c} \cos(2ky)}. \quad (11)$$

Here C^+ is the integration constant. Plot of concentration for different values of parameter $\gamma v_0 U_0 / (a D_c)$ is shown in Supplementary Fig. S1b. This expression exhibits much sharper peaks and gives a much better agreement with the experiment than the corresponding expression for $\gamma = 0$, Supplementary Fig. S1c.

It is of interest to discuss the possible range of parameters entering the model. The relaxation rate of the director in a cell with a finite anchoring at the substrates can be estimated as

$a \sim 2W_s / \eta h^8$, where $\eta \sim 10 \text{ kg m}^{-1} \text{ s}^{-1}$ is the twist viscosity of DSCG⁴, $h = 2 \times 10^{-5} \text{ m}$ is the cell thickness, $W_s \sim 10^{-6} \text{ J/m}^2$ is the in-plane (azimuthal) surface anchoring coefficient at the bounding plates. Then $a \sim 10^{-2} \text{ s}^{-1}$. For a strongly anchored substrates, the rate is higher, $a \sim \pi^2 K / (\eta h^2) \sim 3 \times 10^{-2} \text{ s}^{-1}$, where K is the average Frank elastic constant of the nematic. The expected active force density $|\mathbf{F}| \sim c U_0 \nabla \hat{\mathbf{n}}$ varies broadly, $|\mathbf{F}| \sim (1 - 100) \text{ N/m}^3$, given the range of concentrations $c \sim (1 - 10) \times 10^{14} \text{ m}^{-3}$ and force dipole strength U_0 ; here $|\nabla \hat{\mathbf{n}}| \sim 10^4 \text{ m}^{-1}$ is the typical director gradient. The coefficient γ and the ratio γ / a can vary in an extremely wide range. The minimum is zero, corresponding to the situation when the director anchoring by a bacterium is negligibly weak and when the associated hydrodynamic force dipole does not couple to the director field. The upper limit of γ / a is restricted by the condition $\gamma |\mathbf{F}| / a < 1$, i.e., $\gamma / a < (10^{-2} - 1) \text{ m}^3 / \text{N}$. It is expected that in the dilute regime, when the nematic director and the bacteria follow the pre-inscribed pattern, γ / a is near the upper limit; in simulations presented in Fig. 2d we use $\gamma / a = (2 - 5) \times 10^{-2} \text{ m}^3 / \text{N}$. The combination $\gamma v_0 / (a D_c) \sim (10^4 - 10^5) \text{ m}^2 / \text{N}$, since $v_0 = 10^{-5} \text{ m/s}$, $D_c = 10^{-11} \text{ m}^2 / \text{s}$. Therefore, $\gamma v_0 U_0 / (a D_c) \sim (10^{-14} - 10^{-12}) \text{ m}^3$. In the center of splay region the bacterial concentration c reaches the value of $c_{\text{max}} \sim 10^{15} \text{ m}^{-3}$. Therefore, the product $\gamma v_0 U_0 c_{\text{max}} / (a D_c) > 1$. In the concentrated system with the jets following the already distorted director and wavering into the regions with bend deformations, the destabilizing action of the active force is elastically suppressed; this effectively diminishes γ / a , thus in the simulations of jets in Fig. 3h,i we use a much smaller γ / a , which produces a good agreement with the experiments. Note that even when $\gamma / a = 0$, the analytical results and the numerical simulations are in a qualitative agreement with the experimental data on concentration distribution, see, for example, Fig. 2d.

Advection-diffusion computational model for living nematic. To investigate the experimentally observed undulations we used a 2D computational model that combines Edwards-Beris description of nematic liquid crystal (LC) with advection-diffusion bacterial dynamics, see^{9,10}:

$$(\partial_t + \mathbf{v}_f \cdot \nabla) \mathbf{Q} - \mathbf{S} - \Gamma \mathbf{H} + \mathbf{F}_{\text{exter}} = 0, \quad (12)$$

$$\nabla \cdot (\boldsymbol{\sigma}_s + \boldsymbol{\sigma}_a + \boldsymbol{\sigma}_{\text{visc}} + \boldsymbol{\sigma}_{\text{act}} - p \mathbf{I}) - \zeta \mathbf{v} = 0. \quad (13)$$

Eq. (12) describes evolution of the tensorial nematic order parameter \mathbf{Q} , where \mathbf{v}_f is fluid velocity, tensor \mathbf{S} describes alignment with the fluid flow, \mathbf{H} is molecular field, Γ is director relaxation rate, $\mathbf{F}_{\text{exter}}$ describes director alignment due to wall anchoring (nematic patterning), and \mathbf{I} is the identity tensor. Eq. (13) is linear momentum balance, where $\boldsymbol{\sigma}_s$ is symmetric and $\boldsymbol{\sigma}_a$ is antisymmetric elastic contributions, $\boldsymbol{\sigma}_{\text{visc}}$ is viscous contribution, $\boldsymbol{\sigma}_{\text{act}}$ is active stress that depends on bacterial concentration, p is fluid pressure, and the term $-\zeta \mathbf{v}_f$ is viscous friction term. Equations (12) and (13) are complemented by two evolution equations for bacterial concentrations c^\pm , Eq. (3), and the full coupled partial differential equation (PDE) system consists of four equations and four unknowns: \mathbf{Q} , \mathbf{v}_f , c^+ , c^- .

The continuum Edwards-Beris description is valid for dilute regime when bacteria do not perturb significantly the properties of liquid crystal medium. In our model we also assume that bacteria always swim parallel to the nematic director: $\varphi = \theta$ for c^+ or $\varphi = \theta + \pi$ for c^- population, where φ is bacterial and θ is nematic orientation angles. This assumption is justified by experimental evidence and analytical estimates of the relevant timescales⁹. Our two-population advection-diffusion description is valid for apolar bacterial interactions, since two bacteria that swim in opposite direction can pass each other without a collision on slightly different heights.

The resulting system of PDEs (3, 6, 7) is nondimensionalized, transformed into a system of scalar equations and numerically integrated on Graphical Processor Units. In this work we make only a few minor modifications of the model described in⁹:

- We incorporated nematic patterning using the term $\mathbf{F}_{\text{exter}}$ in Eq. (12). As in⁹, we used the following expression:

$$\mathbf{F}_{\text{exter}} = 4 \xi_{\text{an}} \mathbf{Q} \mathbf{R}_{\pi/2} \text{Tr} \left[\mathbf{Q} \left(\hat{\mathbf{m}} \hat{\mathbf{m}} - \frac{\mathbf{I}}{2} \right) \mathbf{R}_{\pi/2} \right]. \quad (14)$$

Where ξ_{an} controls the alignment strength, $\hat{\mathbf{m}}$ is the alignment direction, $\mathbf{R}_{\pi/2}$ is the rotation matrix. In this work we set $\hat{\mathbf{m}} = (\hat{\mathbf{n}}_0 + 2\gamma \mathbf{F} / a) / |\hat{\mathbf{n}}_0 + 2\gamma \mathbf{F} / a|$, where $\hat{\mathbf{n}}_0$ is the photopatterned direction, Eq. (1), $\mathbf{F} = \nabla \cdot \boldsymbol{\sigma}_{\text{act}}$ is an active stress exerted by bacteria on the nematic, and the ratio

γ / a determines the magnitude of active force alignment, see the main text. Thus, in our framework the nematic director evolves according to Eq. (12) and is allowed to deviate from the photopatterned direction, while the degree of deviation can be controlled by the parameter ξ_{an} .

- The parameters of our model can be found in Table S1. In this work we varied average bacterial concentration c_0 and bacterial diffusion coefficient D_c to match the experimental data. In addition, we reduced the depth-averaging coefficient magnitude to $\zeta = 0.07\eta / h^2$ (compare to ⁹), where η is the effective nematic viscosity, h is the cell thickness. In the DSCG, the bending viscosity is much smaller than twist and splay viscosities ⁴, which reduces the effective viscosity in the expression for depth-averaging term. The value 0.07 was chosen by fitting our model to the experimental data ².
- In our two-populational bacterial model (c^+ swims parallel and c^- swims antiparallel to the nematic) there was an issue near the places with vertical nematic orientation ($\theta = \pi / 2$), where the vector nematic angle is discontinuous (although the nematic director is continuous). To address this issue in ⁹, we relabeled c^\pm concentrations in the detected problematic regions. In this work the nematic direction is approximately given by equation (1), and it is possible to introduce a continuous nematic vector orientation (Fig. 1b). This is achieved by changing $\theta \in (-\pi / 2; \pi / 2]$ to $\theta \in (3\pi / 2; 2\pi]$ in the adjacent regions, separated by bending bands. With the continuous nematic vector angle there is no need for relabeling c^\pm .
- The existence of symmetric nonzero vertical components of the velocity in the simulations, clearly visible in Fig. 2h, comes from the fact that the bacteria from different concentration subsets would converge into splay regions along the positive or negative y direction, thus, acquiring a small positive or negative v_y component. However, the simulations yield no net flows along the y -axis, in agreement with the experiment.

Table S1. Advection-diffusion computational model parameters.

Parameter	Value
Parameters of LC	
Elastic constant, K (pN)	10
Ericksen number, E_r	3.75

Relaxation rate, Γ (m s/kg)	0.1
Isotropic viscosity, η (kg m ⁻¹ s ⁻¹)	0.5
Wall anchoring strength, ξ_{an} (s ⁻¹)	0.3
Cell thickness, h (μm)	20
Aspect ratio parameter, ξ	0.9
Landau – de Gennes coefficient, C_a (N/m ²)	0.4
Landau – de Gennes coefficient, C_b (N/m ²)	0.8
Depth-averaging coefficient, ζ	$0.07\eta / h^2$
Parameters for bacterial transport	
Bacterial length, l_b (μm)	5
Bacterial speed, v_0 ($\mu\text{m/s}$)	10
Average bacterial concentration, $\langle c \rangle$ (m ⁻³)	$(0.3 - 5) \times 10^{14}$
Reversal time, τ (s)	60, 600, ∞
Concentration diffusion, D_c ($\mu\text{m}^2/\text{s}$)	10
Magnitude of bacterial dipole, U_0 (N m)	10^{-17} , 10^{-16}
Parameter γ / a (m ³ /N)	0 – 0.1

Bending instability in the cell with uniform alignment. The uniformly aligned cell with $\hat{\mathbf{n}}_{\text{uniform}} = (1, 0, 0)$ being oriented along horizontal x -axis was used to measure the critical concentration above which the bending instability occurs (Supplementary Fig. S2a and Supplementary Video 2). The thickness of the cell and bacteria activity was chosen to be the same as in patterned cells. We focused on the region where the local bacterial concentration changes along the vertical y -axis and calculated the concentration of bacteria within a thin band of height $\Delta y = 5 \mu\text{m}$. From the time averaged concentration distribution of bacteria along the y -axis

(Supplementary Fig. S2b,c) we find the critical concentration after which the bending instability sets in, in the horizontal band between 100 and 250 μm , to be $c_u^{\text{uniform}} \approx 0.9 \times 10^{14} \text{ m}^{-3}$.

Computational model for two-phase continuum description. To check whether the collective hydrodynamic interactions between the active particles at the dense bacterial concentration limit can affect the focusing behavior, we also introduce a generic active nematic two-phase model. In this model, we adopt a coarse-grained model of the bacteria and show that the focusing can be interpreted in terms of the active stresses they exert once their relative alignment is controlled by the patterned substrate.

We use numerical simulations of active nemato-hydrodynamics to solve for the total density ρ and the fluid velocity \mathbf{v}_f . The orientational order of the bacteria is described by the nematic tensor $\mathbf{Q}_b = \frac{dq}{d-1} \left(\hat{\mathbf{n}}_b \hat{\mathbf{n}}_b - \frac{\mathbf{I}}{d} \right)$, where q denotes the magnitude of the orientational order, d is the dimension, and $\hat{\mathbf{n}}_b$ is the director of the bacteria¹¹. This nematic tensor obeys¹²

$$(\partial_t + \mathbf{v}_f \cdot \nabla) \mathbf{Q}_b - \mathbf{s}_b = \Gamma_d \mathbf{H}_b, \quad (15)$$

where Γ_d is the rotational diffusivity and \mathbf{s}_b is the co-rotational advection term that accounts for the impact of the strain rate $\mathbf{E} = \frac{1}{2}(\nabla \mathbf{v}_f^T + \nabla \mathbf{v}_f)$ and vorticity $\mathbf{\Omega} = \frac{1}{2}(\nabla \mathbf{v}_f^T - \nabla \mathbf{v}_f)$ on the director field. This co-rotational advection has the form

$$\mathbf{s}_b = (\lambda \mathbf{E} + \mathbf{\Omega}) \cdot \left(\mathbf{Q}_b + \frac{\mathbf{I}}{3} \right) + \left(\mathbf{Q}_b + \frac{\mathbf{I}}{3} \right) \cdot (\lambda \mathbf{E} - \mathbf{\Omega}) - 2\lambda \left(\mathbf{Q}_b + \frac{\mathbf{I}}{3} \right) (\mathbf{Q}_b : \nabla \mathbf{v}_f), \quad (16)$$

where the alignment parameter λ is related to the shape of the active particles with $\lambda > 0$ for rod-like particles. The relaxation of the orientational order is controlled by the molecular field

$$\mathbf{H}_b = - \left(\frac{\delta F}{\delta \mathbf{Q}_b} - \frac{\mathbf{I}}{3} \text{Tr} \left(\frac{\delta F}{\delta \mathbf{Q}_b} \right) \right), \quad (17)$$

which models the relaxation towards the minimum of a free energy F .

We introduce an order parameter ϕ to distinguish between the regions where the bacteria are absent $\phi \approx 0$ and present $\phi \approx 1$. The active nematic fluid is mixed with an isotropic fluid, and the amount of each is conserved. We use a scalar parameter ϕ to measure the relative density of

each at a given point. This approach has been used in the past to model growing cell colonies¹³. The assumption here is that we can approximate the concentration of bacteria as uniform and constant in the concentrated bacterial regions.

The order parameter ϕ follows a Cahn-Hilliard equation, $\partial_t \phi + \nabla \cdot (\phi \mathbf{v}_f) = \Gamma_\phi \mu$ where Γ_ϕ is the mobility of the concentration and $\mu = \frac{\delta F}{\delta \phi} - \nabla \cdot \left(\frac{\delta F}{\delta \nabla \phi} \right)$ is the chemical potential which is the functional derivative of the free energy with respect to ϕ .

The total free energy density $F = F_{Q_b} + F_\phi + F_{a,LC}$ contains three components. The first component

$$F_{Q_b} = \frac{A_{Q_b}}{2} (\phi - 0.5) \text{Tr}(\mathbf{Q}_b^2) + \frac{C_{Q_b}}{4} \text{Tr}(\mathbf{Q}_b^2)^2 + \frac{K_{Q_b}}{2} (\nabla \mathbf{Q}_b)^2 \quad (18)$$

is a modified Landau-de Gennes bulk free energy density that couples the ϕ and the nematic order parameter. This ensures that we have nematic ordering in the high ϕ regions. This free energy term also contains the elastic free energy density due to spatial inhomogeneities in the nematic ordering. Here A_{Q_b} , C_{Q_b} , and K_{Q_b} are material constants. The second free energy term

$$F_\phi = \frac{A_\phi}{2} \phi^2 (1 - \phi)^2 + \frac{K_\phi}{2} (\nabla \phi)^2 \quad (19)$$

is a Ginzburg-Landau free energy to allow for phase ordering and surface tension between the active nematic and the surrounding fluid. Here A_ϕ and K_ϕ are again material constants. Lastly, we include the term

$$F_{a,LC} = \frac{W_c}{2} \text{Tr}(\mathbf{Q}_b - \mathbf{Q})^2 \quad (20)$$

to model the effect of the underlying liquid crystal, which has a director field \mathbf{Q} . We contain all bacteria-liquid crystal interactions in this Rapini-Papoular like free energy penalty, which penalizes orientations of the bacteria that are not in alignment with the underlying liquid crystal. This results in a reorientation term in the Beris-Edwards equation. w_c takes the form of an effective anchoring strength which is taken high in our simulations as previous work shows that bacteria quickly relax to the underlying liquid crystal orientation⁹. Since the experiments are performed in a thin-film geometry with the scale of the emergent pattern much larger than the cell thickness, we use a depth-averaged approximation. We also argue that the anchoring of the underlying liquid

crystal to the container walls is sufficiently strong compared to the bacteria-liquid crystal interaction that all perturbations in the liquid crystal are negligible and that \mathbf{Q} is constant in time. This is taken as the imposed pattern due to surface anchoring \mathbf{Q}_0 . This approximation is sufficient to reproduce the experimental observations without taking into account individual swim velocities.

The local density and velocity field obey the incompressible Navier-Stokes equations

$$\nabla \cdot \mathbf{v}_f = 0, \quad (21)$$

$$\rho (\partial_t + \mathbf{v}_f \cdot \nabla) \mathbf{v}_f = \nabla \cdot \mathbf{\Pi}, \quad (22)$$

where $\mathbf{\Pi}$ is the generalized stress tensor that includes both nematic, active and capillary contributions, in addition to the viscous stress $\mathbf{\Pi}^{\text{visc}} = 2\eta \mathbf{E}$, where η is the viscosity. The stress due to elastic contributions arising from nematic ordering of the bacteria is

$$\begin{aligned} \mathbf{\Pi}^{\text{el},\alpha} = & -P \mathbf{I} + 2\lambda \left(\mathbf{Q}_b + \frac{\mathbf{I}}{3} \right) (\mathbf{Q}_b : \mathbf{H}_b) - \lambda \mathbf{H}_b \cdot \left(\mathbf{Q}_b + \frac{\mathbf{I}}{3} \right) - \lambda \left(\mathbf{Q}_b + \frac{\mathbf{I}}{3} \right) \cdot \mathbf{H}_b \\ & - \nabla \mathbf{Q}_b : \frac{\delta F}{\delta \nabla \mathbf{Q}_b} + \mathbf{H}_b \cdot \mathbf{Q}_b - \mathbf{Q}_b \cdot \mathbf{H}_b, \end{aligned} \quad (23)$$

which includes the bulk pressure P ¹².

We also include capillary stresses $\mathbf{\Pi}^{\text{cap}} = (F - \mu\phi) \mathbf{I} - \nabla \phi \frac{\delta F}{\delta \nabla \phi}$ as we work with a two-component system. Lastly, the active stress accounts for changes in the flow field caused by continual energy injection at the microscopic scale. Activity generates flows for nonzero gradients of \mathbf{Q}_b and takes the form $\mathbf{\Pi}^{\text{active}} = \alpha \mathbf{Q}_b$ ¹⁴. The activity parameter α determines the strength of the active flows with negative and positive values denoting extensile and contractile fluids, respectively. It represents the local average energy injection per unit area of the bacteria. This means that it should scale with the concentration of bacteria. In our simulations, we take this parameter to be constant in space and time, as we previously approximated the bacterial density to be constant in the high concentration regimes. The equations of active nemato-hydrodynamics are solved using a hybrid lattice Boltzmann scheme.

In the simulations, the free energy parameters are $A_{\mathbf{Q}_b} = -0.1$, $C_{\mathbf{Q}_b} = 1.2$, $K_{\mathbf{Q}_b} = 0.025$, $A_\phi = 0.05$, and $K_\phi = 0.025$. The tumbling parameter λ is set to 0.3 and the viscosity $\eta = 0.667$. Unless otherwise states, the activity α is -0.003 . All parameters are in lattice Boltzmann units, where the density, lattice size and time step are taken as unity.

Expanding two-phase continuum description to dynamically evolving background LC. The two-component model, as presented above, assumes that the underlying LC order \mathbf{Q} and the patterned surface \mathbf{Q}_0 have the same stationary orientation. This is valid in the limit when the alignment of the passive LC to the substrate is infinitely strong and as such the bacteria-induced flow does not modify underlying LC orientation. We can relax this approximation to allow for realignment of the LC ordering \mathbf{Q} by introducing an additional Beris-Edwards equation⁸

$$(\partial_t + \mathbf{v}_f \cdot \nabla) \mathbf{Q} - \mathbf{S} = \Gamma_d \mathbf{H}, \quad (24)$$

where the LC orientation \mathbf{Q} is coupled to the fluid flow \mathbf{v}_f caused by the LC and the bacterial interactions in Eq. (22), with an additional elastic stress from the LC:

$$\Pi^{el} = -P\mathbf{I} + 2\lambda \left(\mathbf{Q} + \frac{\mathbf{I}}{3} \right) (\mathbf{Q} : \mathbf{H}) - \lambda \mathbf{H} \cdot \left(\mathbf{Q} + \frac{\mathbf{I}}{3} \right) - \lambda \left(\mathbf{Q} + \frac{\mathbf{I}}{3} \right) \cdot \mathbf{H} - \nabla \mathbf{Q} : \frac{\delta F}{\delta \nabla \mathbf{Q}} + \mathbf{H} \cdot \mathbf{Q} - \mathbf{Q} \cdot \mathbf{H}. \quad (25)$$

Furthermore, the molecular field

$$\mathbf{H} = - \left[\frac{\delta F}{\delta \nabla \mathbf{Q}} - \frac{\mathbf{I}}{3} \text{Tr} \left(\frac{\delta F}{\delta \nabla \mathbf{Q}} \right) \right], \quad (26)$$

is modified by expanding the free energy to $F = F_{\mathbf{Q}_b} + F_{\mathbf{Q}} + F_{\phi} + F_{a,LC} + F_{LC,S}$. Here, $F_{\mathbf{Q}}$ is a generic Landau-de Gennes bulk free energy for the background LC:

$$F_{\mathbf{Q}} = \frac{A_{\mathbf{Q}}}{2} (\phi - 0.5) \text{Tr}(\mathbf{Q}^2) + \frac{C_{\mathbf{Q}}}{4} \text{Tr}(\mathbf{Q}^2)^2 + \frac{K_{\mathbf{Q}}}{2} (\nabla \mathbf{Q})^2, \quad (27)$$

where we have used the same free energy parameters as for the bacterial order parameter, \mathbf{Q}_b , for convenience. Lastly, we introduce the free energy term

$$F_{LC,S} = \frac{W_s}{2} \text{Tr}(\mathbf{Q} - \mathbf{Q}_0)^2 \quad (28)$$

to model the reorientation of the underlying liquid crystal with the substrate \mathbf{Q}_0 , where w_s is the surface anchoring between the LC and the substrate, which should be contrasted to w_e , which was the anchoring strength between the bacterial orientation and the background LC.

Long term observation for the bacteria jets. The short, intermediate and long-term behavior of the bacteria jets shown in Supplementary Video 10; the time evolution of undulated jet length,

width and number of bacteria is illustrated in Supplementary Fig. S6. The undulation persists until the bacteria run out of the oxygen and slow down their activity.

References

- 1 Zhou, S. *et al.* Dynamic states of swimming bacteria in a nematic liquid crystal cell with homeotropic alignment. *New Journal of Physics* **19**, 055006 (2017).
- 2 Zhou, S., Sokolov, A., Lavrentovich, O. D. & Aranson, I. S. Living liquid crystals. *Proc Natl Acad Sci USA* **111**, 1265-1270 (2014).
- 3 Smith, C. J. & Denniston, C. Elastic response of a nematic liquid crystal to an immersed nanowire. *Journal of Applied Physics* **101**, 014305 (2007).
- 4 Zhou, S. *et al.* Elasticity, viscosity, and orientational fluctuations of a lyotropic chromonic nematic liquid crystal disodium cromoglycate. *Soft Matter* **10**, 6571-6581 (2014).
- 5 Park, H. S., Kang, S. W., Tortora, L., Kumar, S. & Lavrentovich, O. D. Condensation of self-assembled lyotropic chromonic liquid crystal sunset yellow in aqueous solutions crowded with polyethylene glycol and doped with salt. *Langmuir* **27**, 4164-4175 (2011).
- 6 Nazarenko, V. G. *et al.* Surface alignment and anchoring transitions in nematic lyotropic chromonic liquid crystal. *Phys Rev Letters* **105**, 017801 (2010).
- 7 Collings, P. J., van der Asdonk, P., Martinez, A., Tortora, L. & Kouwer, P. H. J. Anchoring strength measurements of a lyotropic chromonic liquid crystal on rubbed polyimide surfaces. *Liquid Crystals* **44**, 1165-1172 (2017).
- 8 Vilfan, M. & Copic, M. Temperature dependence of azimuthal anchoring strength measured by dynamic light scattering. *Mol Cryst Liq Cryst* **375**, 155-164 (2002).
- 9 Genkin, M. M., Sokolov, A., Lavrentovich, O. D. & Aranson, I. S. Topological defects in a living nematic ensnare swimming bacteria. *Phys Review X* **7**, 1-14 (2017).
- 10 Genkin, M. M., Sokolov, A. & Aranson, I. S. Spontaneous topological charging of tactoids in a living nematic. *New Journal of Physics* **20**, 043027 (2018).
- 11 Gennes, P. G. d. & Prost, J. *The physics of liquid crystals*. (Clarendon Press, 1993).
- 12 Beris, A. N. & Edwards, B. J. *Thermodynamics of Flowing Systems: With Internal Microstructure*. (Oxford University Press, 1994).
- 13 Doostmohammadi, A., Thampi, S. P. & Yeomans, J. M. Defect-Mediated Morphologies in Growing Cell Colonies. *Phys Rev Letters* **117**, 048102 (2016).
- 14 Aditi Simha, R. & Ramaswamy, S. Hydrodynamic fluctuations and instabilities in ordered suspensions of self-propelled particles. *Phys Rev Letters* **89**, 058101 (2002).

Supplementary figures

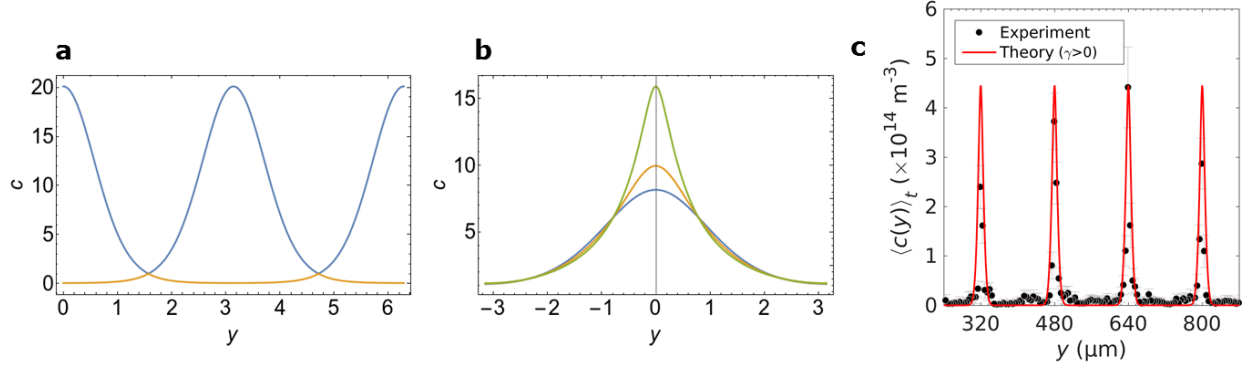


Fig. S1. Concentration distribution from advection diffusion model. **a**, Distributions of c^{right} (blue), c^{left} (orange) as a function of y for $k = 1$, $v_0 / D_c = 3 \text{ m}^{-1}$, and $\gamma = 0$. **b**, Distributions of c^+ for $k = 1$, $C^+ = 3 \text{ m}^{-3}$, $v_0 / D_c = 1 \text{ m}^{-1}$ and for $\gamma = 0$ (blue), $\gamma / a = 0.02 \text{ m}^3/\text{N}$ (orange) and $\gamma / a = 0.04 \text{ m}^3/\text{N}$ (green). **c**, Distribution of the bacteria concentration obtained from the experiment and theoretical curve for $L = 160 \mu\text{m}$, $\gamma / a = 0.5 \times 10^{-3} \text{ m}^3/\text{N}$, $v_0 = 10 \mu\text{m/s}$, $D_c = 10 \mu\text{m}^2/\text{s}$, $C_0 = 1.23 \times 10^{-8} \text{ m}^{-3}$.

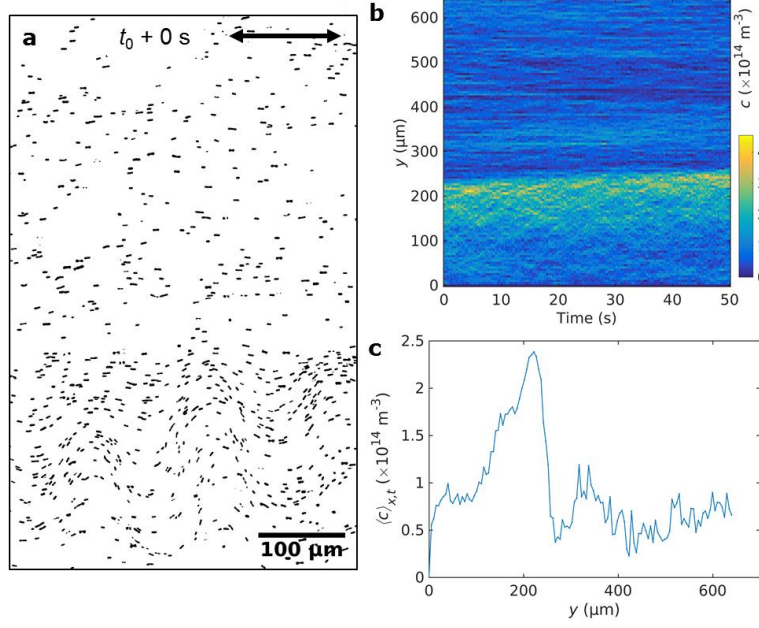


Fig. S2. Bacteria in uniform nematic $\hat{n}_{\text{uniform}} = (1, 0, 0)$ (cell thickness $20 \mu\text{m}$). **a**, Enhanced contrast microscopic image of bacteria swimming through uniformly aligned nematic cell (orientation axis is given by double-headed arrow) with a concentration gradient. Bacteria exhibit both uniform swimming (top part) and bending instability (bottom part). **b**, Kymograph of the time evolution of bacteria concentration along y -axis with the length step $\Delta y = 5 \mu\text{m}$ and time step 0.5 s . **c**, Averaged concentration over time (50 s) and width of the image. Bacteria concentration at which the undulation occurs, is $c_u^{\text{uniform}} \approx 0.9 \times 10^{14} \text{ m}^{-3}$, much lower than the threshold concentration for the undulation of condensed jets in patterned splay-bend cells, $c_u^{\text{s-b}} \approx 11.8 \times 10^{14} \text{ m}^{-3}$.

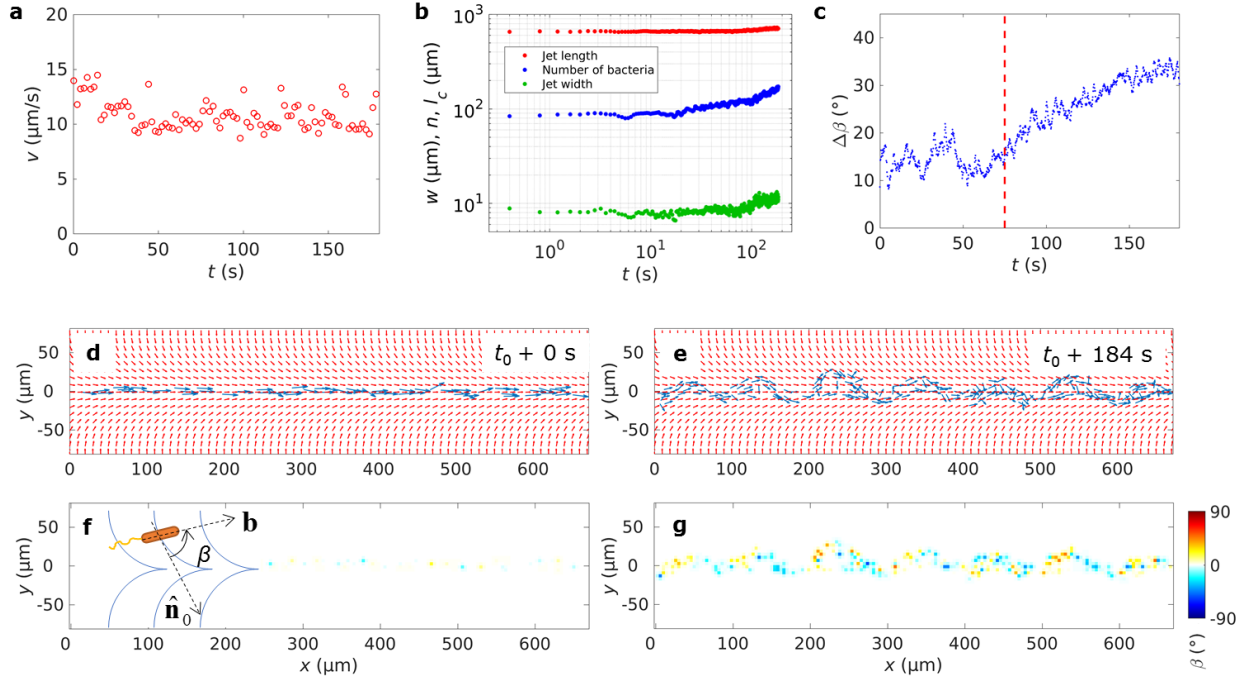


Fig. S3. Undulation of a bacterial jet in a concentrated dispersion $\langle c \rangle \approx 1.5 \times 10^{14} \text{ m}^{-3}$ in a patterned cell of thickness $20 \text{ } \mu\text{m}$. **a**, Average bacteria speed in the developing undulation. **b**, Time evolution of the jet contour length, width and number of bacteria. **c**, Standard deviation of angle β between the bacteria body axes and the director \hat{n}_0 imposed at the substrates, as a function of time. **d**, Pre-imposed director (red arrows) and bacterial axes (blue arrows) in a uniform jet. **e**, The same for an undulating jet. **f**, Definition of the angle β between the bacteria and \hat{n}_0 . **g**, Map of the angle β for the undulating jet shown in part e.

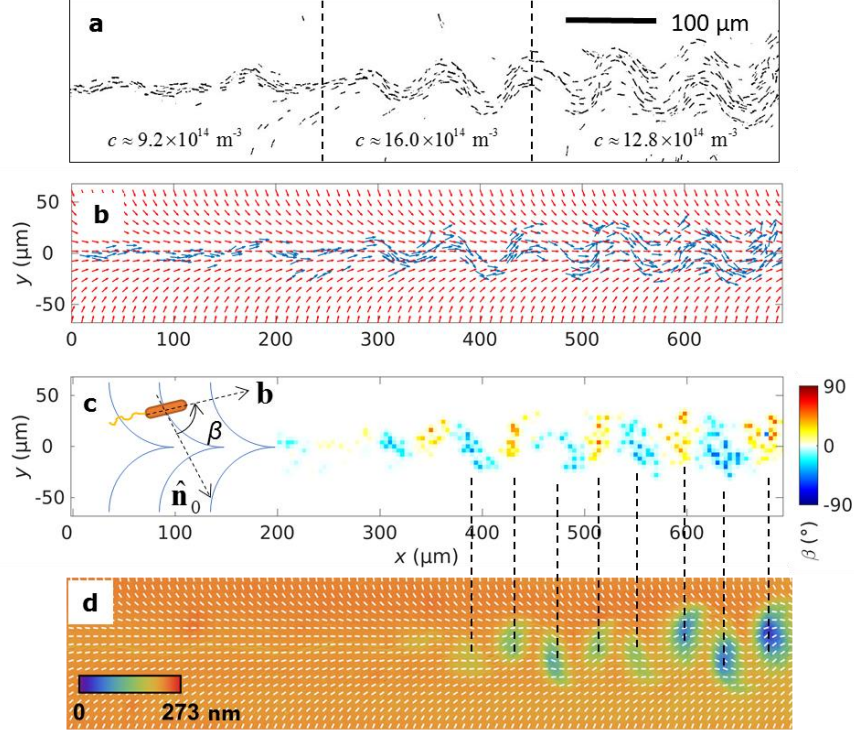


Fig. S4. Undulation instability of a polar jet in the highly concentrated dispersion, $\langle c \rangle \approx 1.5 \times 10^{14} \text{ m}^{-3}$, imaged by PolScope in a $10 \mu\text{m}$ thick cell. **a**, Enhanced contrast microscopic snapshots of bacteria in splay regions of the pattern exhibiting a transition from a rectilinear jet to an undulating jet as the local concentration of bacteria increases thanks to the swimmers joining the jet from the neighboring bend regions. Local concentration is calculated for each region of the jet, using its local width and contour length. **b**, Bacteria body axes (blue arrows) and pre-inscribed \hat{n}_0 (red arrows) for the jet in part **a**. **c**, Map of the angle β between the bacteria and the pre-imposed director. **d**, Optical retardation and the apparent director field for the undulating instability as visualized by PolScope. The scale shows pseudocolors that correspond to the optical retardance of the cell. Low-retardance regions correspond to the twist of the director caused by bacteria in the undulating jet; in these regions, the director field cannot be determined accurately by PolScope.

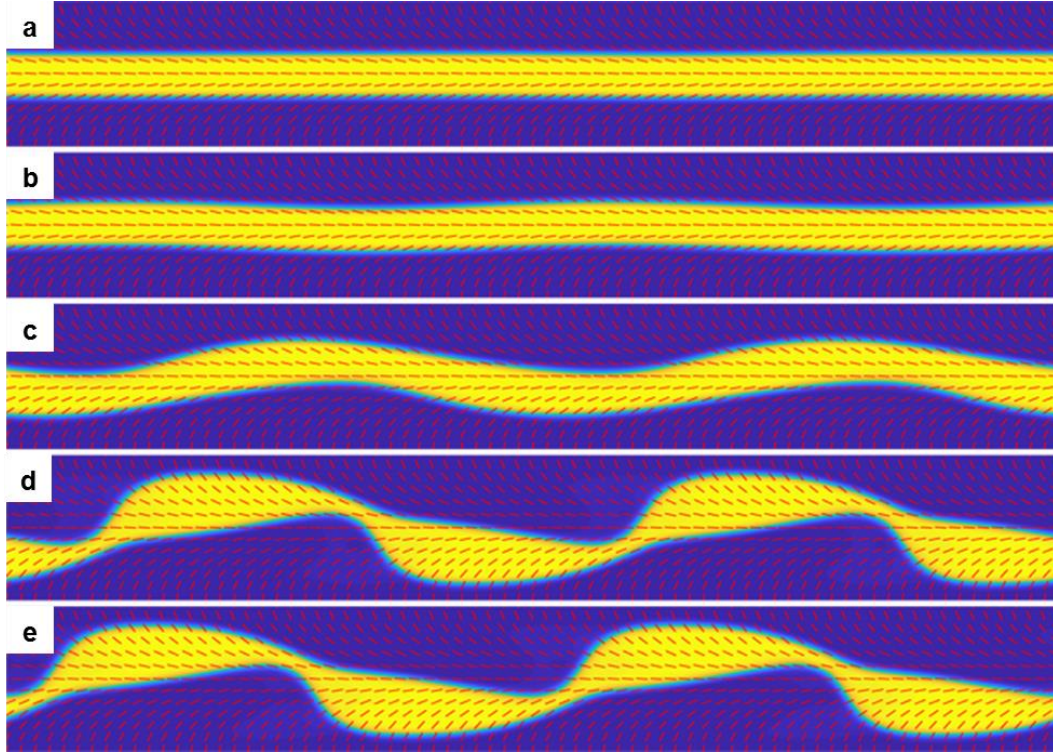


Fig. S5. Simulation results of the extended two-phase model where the underlying LC (red solid lines) evolution is solved over time. Results showing undulation for the alignment strength between the bacteria and background LC $w_c = 0.004$, and alignment strength between the LC and the substrate $w_s = 0.1$. Snapshots are taken respectively for dimensionless simulation time t : **(a)** 0.5×10^4 , **(b)** 1.5×10^5 , **(c)** 2.5×10^5 , **(d)** 3.5×10^5 , **(e)** 4.5×10^5 .

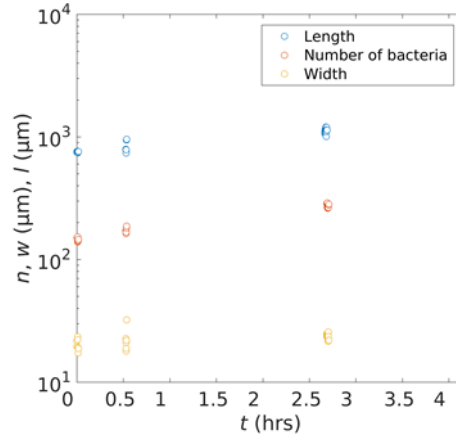


Fig. S6. Time evolution of the number of bacteria n , width and total length of the undulated bacterial jets over extended period of time (> 2 hours).

Supplementary videos

Video 1. Bacterial polar jets focused by the patterned “c” director field in the splay regions, moving from left to right. Bacteria moving in the opposite direction are realigned by experiencing a U-turn in bend regions. Contrast enhanced bright field microscopic images.

Video 2. Swimming bacteria in the uniformly aligned cell of $20\text{ }\mu\text{m}$ with the gradient of bacterial concentration. The lower part of the sample with an elevated concentration of bacteria exhibits a bend instability; in the upper part, the swimmers follow the rectilinear trajectories imposed by the uniform director.

Video 3. Rectilinear jets experience undulations when the concentration of bacteria exceeds some threshold. The amplitude of undulations is stabilized by the underlying pre-imposed patterned director. Note that a small fraction of bacteria swim in the direction opposite to the jet. Contrast enhanced bright field microscopic images.

Video 4. Advection-diffusion simulation of bacterial jets and onset of their undulations. Left panel: variation of concentration of bacteria with time (shown by pseudocolors) and emergence of undulation as the concentration of bacteria increases; black ticks map the director of the passive nematic. Central and right panels: concentration (shown by pseudocolors) and total bacterial velocity fields in the lab frame (shown by black arrows) for c^+ and c^- populations of bacteria.

Video 5. Two-phase simulation of jet formation by extensile swimmers in splay region. The high bacterial concentration is denoted by yellow; the depleted region is blue. The background liquid crystal orientation is shown by red solid lines.

Video 6. Two-phase simulation showing the undulating jet of extensile active fluid. The high bacterial concentration is denoted by yellow; the depleted region is blue. The undulation is stabilized by the underlying passive liquid crystal, marked by red solid lines.

Video 7. Transport of single glass microspheres by the rectilinear bacterial jet moving from left to right in the splay region of the c-stripe patterned director.

Video 8. Transport of a chain of six glass microspheres by the rectilinear bacterial jet moving from left to right in the splay region of the c-stripe patterned director.

Video 9. Transport of micro-particle by an undulating bacterial jet.

Video 10. Snapshots of the bacteria jets at short, intermediate and long ($> 2\text{hr}$) periods of time.